Carbon-based electronics

The semiconductor industry has been able to improve the performance of electronic systems for more than four decades by making ever-smaller devices. However, this approach will soon encounter both scientific and technical limits, which is why the industry is exploring a number of alternative device technologies. Here we review the progress that has been made with carbon nanotubes and, more recently, graphene layers and nanoribbons. Field-effect transistors based on semiconductor nanotubes and graphene nanoribbons have already been demonstrated, and metallic nanotubes could be used as high-performance interconnects. Moreover, owing to the excellent optical properties of nanotubes it could be possible to make both electronic and optoelectronic devices from the same material.

PHAEDON AVOURIS*, ZHIHONG CHEN AND VASILI PEREBEINOS

IBM T. J. Watson Research Center, Yorktown Heights, New York, 10598, USA
***e-mail: avouris@us.ibm.com**

In the last few decades we have witnessed dramatic advances in electronics that have found uses in computing, communications, automation and other applications that affect just about every aspect of our lives. To a large extent these advances have been the result of the continuous miniaturization or 'scaling' of electronic devices, particularly of silicon-based transistors, that has led to denser, faster and more power-efficient circuitry. Obviously, however, this device scaling and performance enhancement cannot continue forever; a number of limitations in fundamental scientific as well as technological nature place limits on the ultimate size and performance of silicon devices.

The realization of the approaching limits has inspired a worldwide effort to develop alternative device technologies. Some approaches involve moving away from traditional electron transport-based electronics: for example, the development of spin-based devices. Another approach, on which we focus here, maintains the operating principles of the currently used devices, primarily that of the field-effect transistor, but replaces a key component of the device, the conducting channel, with carbon nanomaterials such as one-dimensional (1D) carbon nanotubes (CNT) or two-dimensional (2D) graphene layers, which have superior electrical properties[1]. Furthermore, semiconducting carbon nanotubes are direct bandgap materials providing an ideal system to study optics and optoelectronics in one dimension and explore the possibility of basing both electronics and optoelectronic technologies on the same material.

In this article we examine the electronic structure, electrical transport and optoelectronic properties of CNTs, with a focus on the physical phenomena involved. We discuss briefly the emerging area of study involving single graphene layers and narrow graphene nanoribbons (GNRs). We analyse the switching mechanism and characteristics of single-CNT field-effect transistors (FETs), GNR FETs and efforts towards device integration. We also describe the principles of simple CNT optoelectronic devices such as electroluminescent light emitters and photodetectors.

ELECTRONIC STRUCTURE

Graphite is a well-known allotropic form of carbon composed of layers of sp^2-bonded carbon atoms in a honeycomb arrangement (Fig. 1a). The different carbon layers in graphite interact weakly, primarily by van der Waals forces. This interaction produces a small valence and conduction band overlap of about 40 meV, which makes graphite overall a semi-metal. The electronic structure of graphene, an individual layer of graphite, was first discussed by P. R. Wallace in 1947 (ref. 2). There are about 3 million layers in a millimetre thickness of graphite and the experimental study of graphene has been thwarted by the difficulty of isolating and studying this single atomic layer.

Recently, however, graphene became the object of intense experimental study when it was realized that single layers, or a few layers, could be produced relatively easily by mechanical exfoliation of graphite[3], or by heating SiC (ref. 4). Figure 1b shows the peculiar single-particle band structure of this 2D material. The linear dispersion at low energies makes the electrons and holes in graphene mimic relativistic particles that are described by the Dirac relativistic equation for particles with spin 1/2, and they are usually referred to as Dirac Fermions. Their dispersion, $E_{2D} = \hbar v_F \sqrt{k_x^2 + k_y^2}$, is analogous to that of photons, $E_k = \hbar ck$, but with the velocity of light c replaced by $v_F \approx 10^6$ m s^{-1}, the Fermi velocity. Thus, electrons and holes in graphene have zero effective mass and a velocity that is about 300 times slower than that of light. This linear dispersion relationship also means that quasi-particles in graphene display properties quite different to those observed in conventional three-dimensional materials, which have parabolic dispersion relationships. For example, graphene displays an anomalous quantum Hall effect and half-integer quantization of the Hall conductivity[5,6]. The quantum Hall effect in graphene can be observed even at room temperature[7].

The electronic structure of CNTs is usually discussed on the basis of the band structure of graphene. The CNT is thought of as being formed by the rolling of a piece of a ribbon of graphene to form a seamless cylinder. To a large extent, the remarkable electrical properties of carbon nanotubes have their origins in the unusual electronic structure of graphene. The rolling process forming the nanotube and the resulting nanotube structure are specified by a pair of integers (n,m) defining the chiral vector

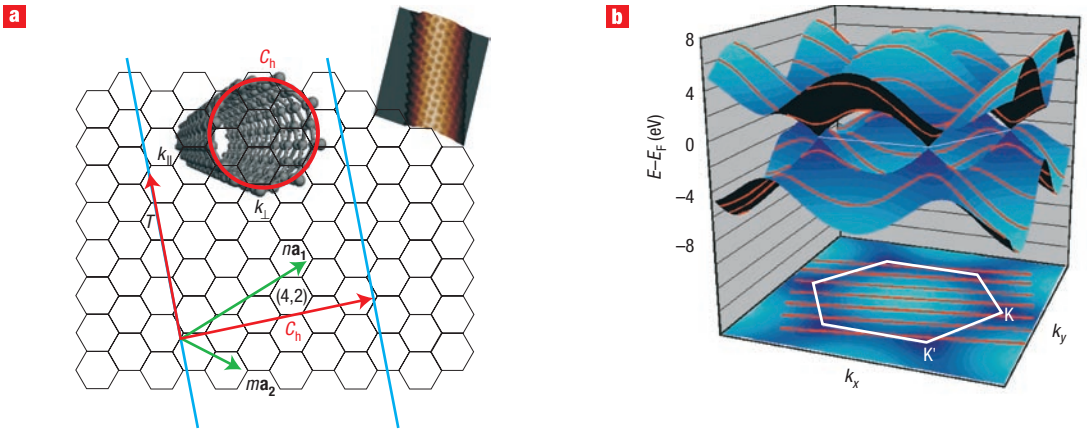

Figure 1 The structure of graphene and carbon nanotubes. **a**, The carbon atoms in a single sheet of graphene are arranged in a honeycomb lattice. A nanotube can be formed by rolling a ribbon of graphene along a chiral vector, C_h, defined by two integers, such as the (4,2) chiral vector shown here. The insets show the definitions of $k_\perp$ and $k_{||}$ (left), and a scanning tunnelling microscope image (right) of a single-walled nanotube. **b**, The band structure (top) and Brillouin zone (bottom) of graphene. The valence band (which is of π-character) and the conduction band (π^*-character) touch at six points that lie at the Fermi energy, but only two of these points — the K and K' points — are inequivalent. At these Dirac points, the density-of-states is zero, so graphene can be considered as a zero-gap semiconductor. At low energies, the dispersion is linear, determined by the conical sections involving the K and K' points. The quantization of the circumferential momentum, $k_\perp$, leads to the formation of a set of discrete energy sub-bands for each nanotube (red parallel lines). The relation of these lines to the band structure of graphene determines the electronic structure of the nanotube. If the lines pass through the K or K' points, the nanotube is a metal: if they do not (as in **b**), the nanotube is a semiconductor. Specifically, (n,n) nanotubes (armchair tubes) are always metallic, and (n,m) nanotubes with $n-m = 3j$, where $j = 1,2,3\ldots$, are nearly metallic with a small, curvature-induced gap that has a $1/d^2$ dependence. Tubes with $n-m \neq 3j$ are semiconductors.

$C_h = n\mathbf{a_1} + m\mathbf{a_2}$ that describes the circumference of the nanotube ($C_h = \pi d_{CNT}$), where $\mathbf{a_1}$ and $\mathbf{a_2}$ are the unit vectors of the graphene honeycomb lattice. The periodic boundary conditions around the circumference of a nanotube require that the component of the momentum along the circumference[8], $k_\perp$, is quantized: $C_h k_\perp = 2\pi\nu$ where ν is a non-zero integer. On the other hand, electron motion along the length of the tube is free and $k_{||}$ is a continuous variable. As explained in Fig. 1a this quantization leads to the formation of metallic and semiconducting nanotubes. In the simple tight-binding model the bandgap of semiconducting nanotubes E_g is given by $E_g = 4\hbar v_F/3d_{CNT} = \gamma(2R_{C\text{-}C}/d_{CNT})$, where γ is the hopping matrix element (~3 eV), $R_{c\text{-}c}$ is the C–C bond length and d_{CNT} is the CNT diameter[8]. Further details on this subject can be found in recent review articles[9,10].

Whereas 2D graphene is a semi-metal, electrons (and holes) can be further confined by forming narrow ribbons, for example by quantizing k_x or k_y. This confinement should open a gap and make the GNR a finite gap semiconductor[4,11–13]. The confinement gap is expected to be inversely proportional to the width W of the GNR, given approximately by: $\Delta E_C \approx 2\pi\hbar v_F/3W$ (refs 13–17). We should note here the differences in confinement quantization in CNTs and GNRs. In a 1D quantum box of width W, quantization requires that $k_\perp = n\pi/W$, thus the allowed energy states are spaced as π/W. In a circular box of circumference C, on the other hand, the requirement is: $k_\perp = 2n\pi/C$ and the states are spaced apart as $2\pi/C$. Thus, qualitatively we expect a larger confinement gap in a CNT than in a GNR with the same confinement dimension. In addition to the difference in the gap value, the electronic states in GNRs are not degenerate, whereas those of CNTs are doubly degenerate. This is due to the difference in the boundary conditions: in a GNR the wavefunction has to vanish at the edges, whereas in a CNT the wavefunction is periodic in the circumference direction.

The above picture of the nanotube electronic structure is a single-electron model that accounts well for many of the CNT ground states properties. Interactions between electrons, however, can be important and can modify, among other properties, the predicted semiconducting bandgaps and can affect the nature of the excited states of the CNTs[18].

NANOTUBE ELECTRICAL PROPERTIES

Individual nanotubes, like macroscopic structures, can be characterized by a set of electrical properties — resistance, capacitance and inductance — which arise from the intrinsic structure of the nanotube and its interaction with other objects. Electrical transport inside the CNTs is affected by scattering by defects and by lattice vibrations that lead to resistance, similar to that in bulk materials. However, the 1D nature of the CNT and their strong covalent bonding drastically affects these processes. Scattering by small angles is not allowed in a 1D material, only forward and backward motion of the carriers. Most importantly the 1D nature of the CNT leads to a new type of quantized resistance related to its contacts with three-dimensional (3D) macroscopic objects such as the metal electrodes[19,20]. The confinement of the electrons in the CNT around its circumference produces a small number of discrete states (modes) that overlap the continuous states of the metal electrodes. This mismatch of the number of states that can transport the current in the CNT and the electrodes leads to a quantized contact resistance, R_Q. The size of the resistance is determined by the number of modes, M, in the CNT that have energies lying between the Fermi levels of the electrodes: $R_Q = h/(2e^2M)$. For a metallic CNT, M=2 so that $R_Q = h/4e^2 = 6.45\ \text{k}\Omega$.

Of course, as well as this quantum resistance there are other forms of contact resistance such as that attributable to the presence of Schottky barriers at metal–semiconducting nanotube interfaces, of which we will speak later, and 'parasitic' resistance, which is simply due to bad contacts. When the only resistance present is the quantum resistance, transport in the CNT is ballistic — that is, no carrier scattering or energy dissipation takes place in the body of the CNT. This is obviously an important transport regime that is uniquely accessible to CNT conductors. The length over which a CNT can behave as a

ballistic conductor depends on its structural perfection, temperature and the size of the driving electric field. In general, ballistic transport can be achieved over lengths typical of modern scaled electronic devices, that is ≤100 nm. At the other extreme, in long CNTs, or at high bias, many scattering collisions can take place and the so-called diffusive limit of transport that is typical of conventional conductors is reached. In this limit the carriers have a finite mobility. However, in CNTs this can be very high — as much as 1,000 times higher than in bulk silicon.

The intrinsic electronic structure of a CNT also leads to a capacitance that is related to its density-of-states — that is, how its energy states are distributed in energy — and it is independent of electrostatics. This quantum capacitance, C_Q, is small — of the order of 10^{-16} F μm^{-1} (ref. 21). In addition to C_Q, a CNT incorporated in a structure has an electrostatic capacitance, C_G, which arises from its coupling to surrounding conductors and as such depends on the device geometry and dielectric structure. In a typical metal oxide semiconductor FET (MOSFET) and in a planar graphene FET, $C_G \approx 1/t_{ins}$, where t_{ins} is the thickness of the gate insulator. In single-CNT FETs, geometry leads to a weaker variation, $C_G \approx 1/\ln(t_{ins})$. C_G and C_Q are coupled in series — that is, $1/C_{total} = 1/C_G + 1/C_Q$ — and therefore the smaller capacitance should dominate. In most experimental CNTFETs, C_G is smaller than C_Q, but in a highly miniaturized CNTFET with a high dielectric-constant insulator, $C_Q \lesssim C_G$ and therefore C_Q can dominate the total capacitance and determine the performance of the device.

Finally, CNTs have inductance, which is a resistance to any changes in the current flowing through them[22]. Again, there is a quantum and a classical contribution. The quantum inductance, usually referred to as kinetic inductance, L_K, is the resistance to the change of the kinetic energy of the electrons of the CNT. It leads to electron velocities that lag in phase with respect to the external driving field and is proportional to the density of states of the CNT. Classical self-inductance depends on the CNT diameter, geometry of the structure and the magnetic permeability of the medium. The total inductance is the sum of the two values, so that the larger inductance, L_K, dominates ($L_K \approx 16$ nH μm^{-1}, $L_C \approx 1$ nH μm^{-1}). In response to an a.c. signal, a CNT behaves like a transmission line owing to its inductance.

SCATTERING MECHANISMS AND TRANSPORT

As we already indicated above, CNTs are unique materials in terms of their long elastic mean free path, which is of the order of a micrometre. In metallic CNTs in particular, the symmetry of the band structure forbids backscattering as long as the carrier energies are below the second sub-band[23]. Long-range Coulomb scattering is ineffective, but a strong, short-ranged potential can lead to backscattering. In general, as the diameter of the CNT increases, the influence of a defect decreases because the influence of the CNT wavefunction is diluted[24]. Transport in graphene has recently been proposed as an example of the Klein paradox[25]: unimpeded penetration of relativistic particles through high and wide potential barriers[26]. Thus, unlike conventional 2D systems where strong disorder leads to Anderson localization, the transparency of the barriers (at least for some angles) in graphene could lead to efficient percolation of localized regions even for E_F close to the Dirac point.

Because elastic scattering in CNTs is weak, inelastic scattering processes determine their transport properties. These processes depend on the energy (applied bias) of the carriers. At low temperatures and low bias, only low-energy acoustic phonons can scatter the electrons, which results in an inverse temperature dependence of the carrier mobility in semiconducting CNTs[27,28], unlike in bulk materials, where acoustic phonon scattering typically leads to a $\sim 1/T^5$ temperature dependence of mobility[29]. The stronger temperature dependence in three dimensions is due to phase-space restrictions and the occurrence of low-angle scattering[29]. In carbon nanotubes, acoustic phonon scattering is predominantly a backscattering event, and the phase-space is nearly temperature independent. Only a small fraction of phonons in the vicinity of the zone centre and zone boundary can effectively participate in the scattering. This is the result of the energy and momentum conservation law requirements and the mismatch in the phonon sound velocity and electron band velocity. The low-field mobility is very high in carbon nanotubes, even at room temperature[30]. This is unlike many other materials, such as III–V semiconductors, which have a very high mobility at low temperatures, but a substantially degraded one at room temperature. The main reason for the uniquely high mobility in carbon nanotubes is the very weak electron–acoustic-phonon coupling and the very large optical phonon energy of about 200 meV.

In addition to the low-energy acoustic phonons, electron (or hole) scattering by the radial breathing mode (RBM) is important in the low bias regime. The RBM phonon energy is inversely proportional to the tube diameter[8], and its energy is comparable to the thermal energy at room temperature for tubes in the diameter range of $d_{CNT} = 1.5$–2.0 nm, which are of interest for electronic applications. As the acoustic mean free path is very long — of the order of a micrometre at room temperature — electrons can be accelerated up to the RBM energy not only thermally, but also by an applied bias of a few V cm^{-1}.

The 1D nature of the electronic states of CNTs leads to van-Hove singularities in the density of states, which in turn are responsible for the non-monotonic dependence of the mobility on band filling[28,30,31]. As the band is filled — by the applied gate potential — the mobility initially increases owing to the loss of available final states for the scattered particles. Once the Fermi level reaches a higher-energy sub-band, an additional scattering channel opens and again lowers the mobility. The inverse diameter dependence of the effective mass and of the electron–phonon coupling strength leads to a quadratic diameter dependence of the mobility[27], which is confirmed experimentally[28].

Unlike acoustic phonon scattering, optical phonon scattering is very strong in carbon nanotubes; optical phonons contract and elongate the C–C bond length and lead to a strong modulation of the electronic structure. However, for electrons to emit an optical phonon, their energies must be larger than the optical phonon energy. This can only be achieved under high bias conditions. Such scattering processes were first observed in metallic tubes[32–34] and later in semiconducting tubes[35]. In metallic tubes, the current was found to saturate at about 25 μA owing to the short optical phonon mean-free-path, of the order of 10–20 nm, whereas in semiconducting CNTs, a velocity saturation was observed[35] in accord with earlier theoretical predictions[27,36].

As the carrier energy increases further, other inelastic processes can take place, in particular, impact excitation[37,38]. The analogous process in bulk semiconductors is impact ionization, where a high-energy electron can lose its energy by scattering to a lower energy state and impact exciting an electron–hole pair. In low-dimensional materials like carbon nanotubes, the electron–hole interaction is very strong, which leads to the formation of excitons with large binding energies (a few tenths of an eV)[39–41]. As a result, in CNTs, impact excitation primarily produces excitons[38]. The impact excitation process is governed by the Coulomb interaction, which is very strong in 1D systems, and indeed calculations suggest that impact excitation processes in CNTs are much more efficient (about four orders of magnitude stronger) than in conventional bulk semiconductors[38].

Unlike in 3D bulk materials, the longitudinal momentum along the tube axis of the produced excitons is nearly zero, whereas the angular momentum is finite. Furthermore, the difference between the impact excitation and the impact ionization rates, neglecting the strong electron–hole interaction in the produced electron–hole pair,

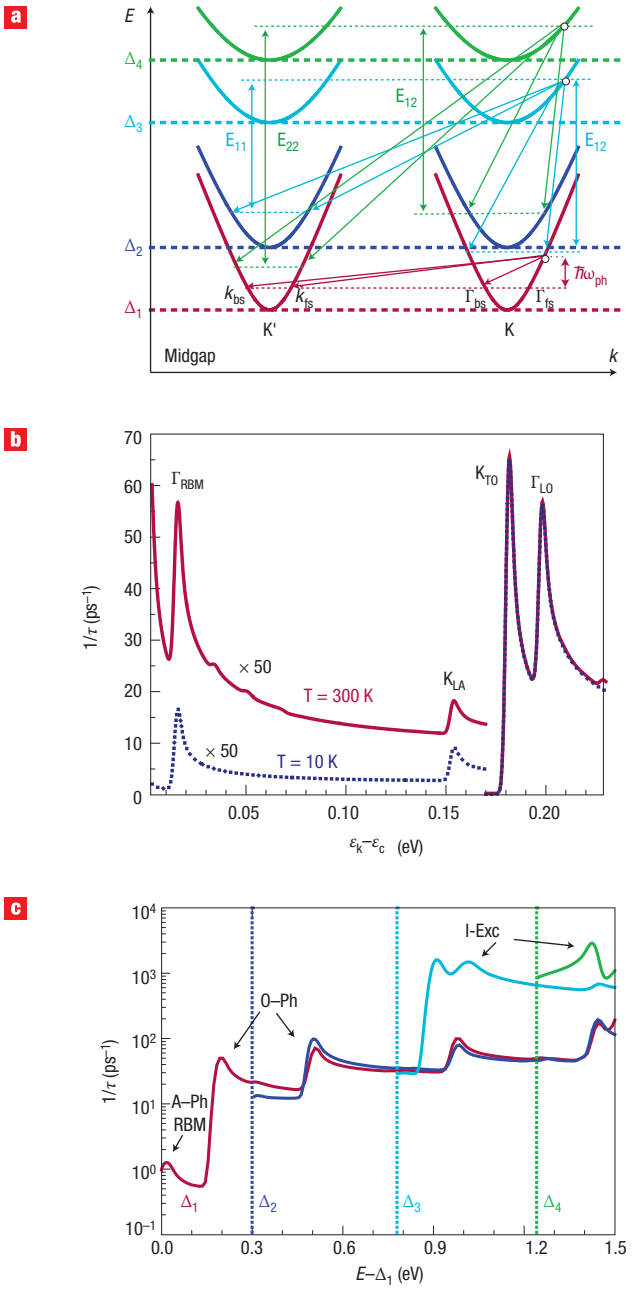

Figure 2 Inelastic scattering in carbon nanotubes. **a**, Schematic illustration of the intra-sub-band (Γ) and inter-sub-band (K) phonon scattering mechanisms (red) and electron impact excitation (blue and green curves) for the first four conduction bands. The different conduction band edges are labelled as Δ_i and the resulting electronic excitations are denoted as E_{ij}. Subscripts bs and fs stand for the back and forward scattering. **b**, Calculated phonon scattering rate for a (25,0) nanotube showing weak acoustic phonon scattering and strong optical phonon scattering. **c**, Calculated inelastic scattering rate for a (19,0) nanotube over a wide carrier energy range. Different colours correspond to the scattering rates of electrons in bands with different circumferential angular momentum. The vertical lines show the bottoms of the conduction bands 2 (blue), 3 (cyan) and 4 (green) with respect to the fundamental band edge Δ_1. Some of the characteristic peaks in the scattering, due to the longtitudinal (LA) acoustic phonons (A-Ph), radial breathing mode (RBM), longitudinal (LO) and transverse (TO) optical phonons (O-Ph) and impact electronic excitation (I-Exc), are labelled. In **b** and **c** the electron scattering rate is shown as a function of the excess energy of the electron above the first conduction-band minimum.

is much higher in carbon nanotubes than in other studied systems. The energy necessary for the electronic excitation is provided by the 'hot' carriers. Conservation of circumferential angular momentum $k_\perp$ plays a critical role in determining the threshold energy, E_{th}, for the onset of impact excitation in CNTs. The carriers are accelerated by the field, but they also lose energy to phonons, particularly to high-energy optical phonons and electronic transitions. This problem can be treated by solving the corresponding Boltzmann equation[38]. It is found that the exciton production rate P (per unit carrier) varies exponentially with the applied field F as $P \approx \exp(-E_{th}/eF\lambda_{op})$, where E_{th} is the excitation threshold and λ_{op} (~20–40 nm) is the electron mean free path due to optical phonon scattering. The energy of the optical phonons is usually efficiently dissipated into the heat bath provided by the substrate. However, in the case of suspended nanotubes, evidence for the existence of a non-equilibrium optical phonon excitation has been presented. This phonon excitation degrades the carrier mobility in CNTs[42,43]. The effect was included in the Boltzmann model by having the optical phonons at different temperatures, T_{op}, while keeping the other phonons at ambient temperature. The resulting exciton production rate could well be fitted by an exponential dependence with an effective temperature, T_{eff} (ref. 38).

In summary, the inelastic scattering rates determining transport properties of carbon nanotubes vary by four orders of magnitude depending on the energy of the electrons and their angular momentum (sub-band index) as shown in Fig. 2. The weakest is the acoustic (primarily RBM) phonon scattering, which has linear temperature dependence. The optical phonon scattering rate, which is two orders of magnitude stronger, is nearly temperature independent. Finally, another two orders of magnitude stronger than the optical phonon scattering is impact excitation. It can only be observed at very large local fields of above ~3×10^4 V cm^{-1}, at which higher energy CNT sub-bands can be populated with the charge carriers. At higher fields CNT dielectric breakdown takes place[44,45].

ELECTRICAL SWITCHING OF CARBON NANOTUBES

Whereas metallic, particularly multiwalled, CNTs offer the possibility of use as high-performance interconnects in very-large-scale integrated systems[46], transport in semiconducting CNTs can be switched 'on' and 'off', which means that semiconducting CNTs can be used as a basis of novel transistors.

The flow of electricity in a semiconductor requires some kind of activation (for example, heating or light absorption) to get the charge carriers over the gap, or modulation of the gap by some external influence such as an applied strain, electric field or magnetic field. The most common mode of switching, which forms the basis of modern microelectronic industry, is by means of an external electric field, in the so-called field-effect transistor. The idea of the FET is quite old, but it was not until 1960 when John Atalla of Bell Laboratories demonstrated the modern form of the FET, the MOSFET. The basic structure involves a channel made of a semiconductor, typically silicon connected to two electrodes: a source (S) and a drain (D). An insulating thin film, usually SiO_2, separates the channel and the source and drain from a third electrode called the gate (G). By applying a voltage at this gate electrode with respect to the source (V_g), we can modulate (switch) the conductance of the semiconducting channel (Fig 3a). The carriers (electrons or holes) travelling from the source to the drain encounter a material- and structure-dependent energy barrier in the bulk of the semiconductor. This barrier is in the conduction band for an electron (n-type semiconductor), or in the valence band for a hole (p-type). The electric field generated by the biased gate, depending on its direction, lowers or raises the barrier and thus changes the conductivity. For example, for electron conduction, application of a positive V_g lowers the barrier, whereas a negative V_g raises it.

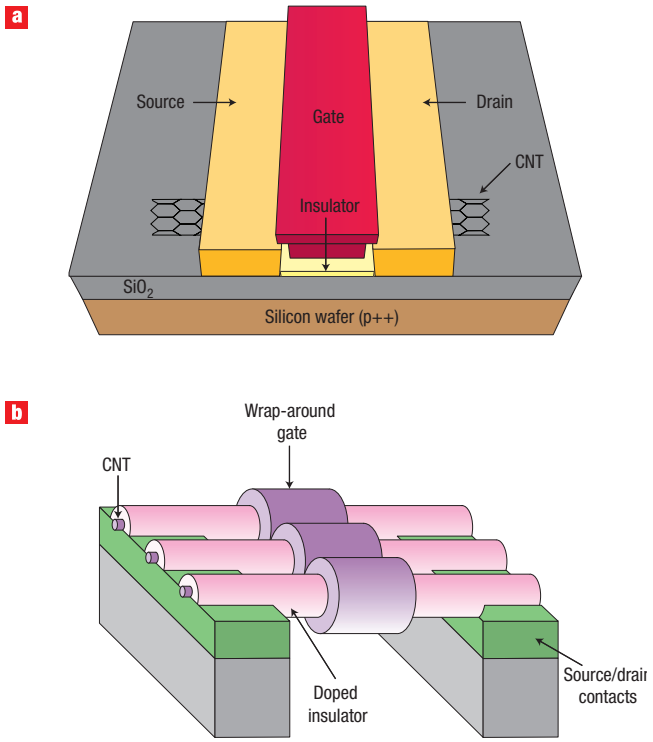

Figure 3 Designs of carbon nanotube field-effect transistors. **a**, Schematic of a top-gated carbon nanotube field-effect transistor. **b**, Schematic of an array of nanotube transistors with wrap-around gates and doped gate extensions (courtesy of P. M. Solomon).

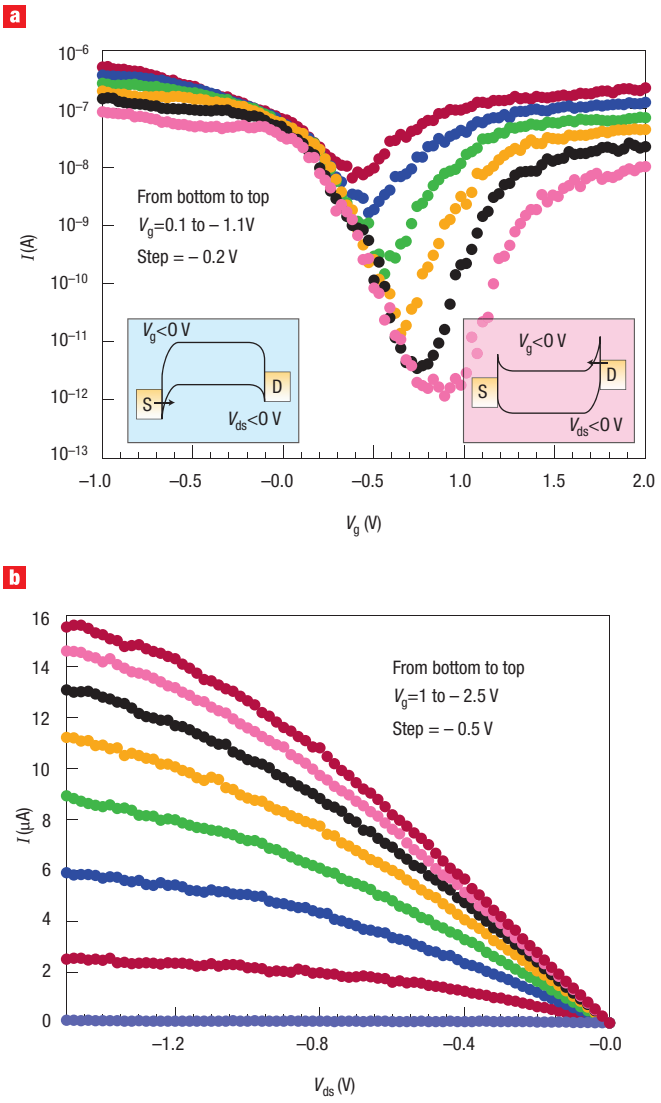

Figure 4 Performance characteristics for a single nanotube transistor. **a**, Ambipolar transfer characteristics (current versus gate voltage): drain bias increases from –0.1 V to –1.1 V in –0.2 V steps. Left inset: schematic of the band structure of a Schottky barrier semiconducting CNT in a FET under negative gate bias. Holes are injected from the source (S). Right inset: under positive gate bias electrons are injected from the drain (D). **b**, Output characteristics (current versus drain bias): gate voltage changes from +1 V (off state) to –2.5 V (on state) in –0.5 V steps.

The first CNTFETs were reported in 1998[47,48]. In a CNTFET the role of the channel is played by one (or more) semiconducting nanotubes. In Fig. 3 we show schematically two different CNTFET structures: a top-gated CNTFET and an array of CNTFETs with 'wrap-around' gates. Typical current–voltage characteristics of a CNTFET are shown in Fig. 4. The atomic and electronic structures of the nanotube give it a number of unique advantages as a FET channel. First, its small diameter (1–2 nm) allows optimum coupling between the gate and the channel, that being the ability of the gate to control the potential of the channel. This is particularly true for the wrap-around gate configuration shown in Fig. 3b. This strong coupling makes the CNT the ultimate 'thin-body' semiconductor system and allows the devices to be made shorter while avoiding the dreaded 'short-channel effects'[49], which basically involve the loss of control of the device by the gate field. The fact that all bonds in the CNT are satisfied and the surface is smooth also has important implications. Scattering by surface states and roughness, which plagues conventional FETs, especially at high V_g values, is absent. Of course, the key advantage is the low scattering in the CNT and the high mobility of the FET channel.

CNTFETs have a number of other differences with conventional MOSFETs. The profile of the energy bands of the CNTFET at a given drain bias, V_{ds}, is determined by V_g and the capacitance of the FET. As we discussed above there are two contributions to the capacitance: C_G and C_Q coupled in series. Now in conventional devices, $C_G<C_Q$ and C_G is the controlling term, but in very small (scaled down) CNTFETs, $C_G \approx C_Q$ or even $C_G>C_Q$ and the quantum capacitance can be dominant. The quantum capacitance has an important consequence on how the gate voltage affects the band profile (energy barrier) of the CNT. In a conventional MOSFET the ability of the gate to control the potential in the channel is limited once V_g exceeds the threshold voltage, V_{th} (ref. 49). Increasing the gate voltage above this value does not change the bands any more because the increased charge pulled into the channel by an increase in V_g pushes the bands back up by electrostatic repulsion. In a C_Q-controlled device, however, the gate can still retain control of the potential in the CNT channel. Higher CNT conduction bands can now be pulled by the gate below the Fermi level of the S, thus contributing to the current[50].

The above discussion on CNTFETs assumed the existence of only one, bulk barrier in the motion of the carriers as in MOSFETs. In MOSFETs, in addition to the channel, the source, drain and gate are also made of heavily doped Si and the contacts are ohmic. This is not generally true for the CNT–metal contacts used in CNT electronics[51–54]. Metals like Au, Ti, Pd and Al are used for the source and drain electrodes. The different work functions of the metal and

the CNT lead to transfer of charge at their interface. The resulting interface dipole produces an energy barrier, the so-called Schottky barrier. The alignment of the Fermi levels of the metal and CNT, and therefore the Schottky barrier height, depend on their respective work functions (Φ), the CNT bandgap and the details of chemical bonding at the interface.

There are two Schottky barriers in a FET; one at the source and another at the drain as shown schematically in the insets of Fig. 4a. As long as one of the barriers is much higher than the other, the FET operates as a unipolar device; that is, it transports one type of carrier: electrons, or holes. For example, a high Φ metal such as Pd could be used to form a nearly barrierless contact for holes[55] (valence band close to the metal Fermi level, E_F), that is to optimize a p-type CNTFET operation, but electron injection at the other end would then experience the maximum barrier of E_g. Correspondingly, a low work-function metal, for example, Al, will optimize electron transport, but will inhibit hole transport. However, typically, carrier transport through the metal-CNT interface is dominated by quantum mechanical tunnelling through the Schottky barrier rather than thermally-activated — thermionic — emission over the Schottky barrier[53,56,57] and, therefore, the thickness of the Schottky barrier becomes critical. In 1D systems like CNTs, the intrinsic screening is weak and the distribution of the potential is determined by the screening provided by the nearby metallic gate[51], and also decreases with increasing d_{CNT}. Therefore, we should expect that, in a thin gate oxide CNTFET, both Schottky barriers can become thin enough to allow, depending on the bias, the injection of either electrons or holes, or of both carriers simultaneously. Such a type of transistor is called ambipolar[52,53,58]. The insets of Fig. 4a show how the application of different gate voltages (V_g) brings about the injection of electrons or holes. We can now understand the I–V_g characteristics of the ambipolar CNTFET shown in Fig. 4a. For a strongly negative or positive V_g, holes or electrons are injected, respectively. However, for V_g values in the vicinity of the current minimum, both electrons and holes contribute to the current, and at $V_g = V_{ds}/2$, the two currents are of equal size[53,58].

Schottky barriers in a CNTFET impact the characteristics of both the 'on' and 'off' states[59]. An important parameter in this regime is the inverse sub-threshold slope, S, that measures the efficiency with which the gate switches the channel, and is defined as $S = (\mathrm{d}\log_{10}I/\mathrm{d}V_g)^{-1}$. In a transistor with ohmic source and drain contacts (as in a conventional Si MOSFET), S is limited by thermionic emission over the channel and is $\approx k_BT/q$ — that is, ~60 meV per decade at 300 K. However, in a transistor with Schottky barriers dominating its transport, S is significantly higher, about 100–150 mV per decade for oxide thickness $t(SiO_2) \lesssim 10$ nm. It is not only the 'on' current of the transistor that is important. The current in the 'off' state is equally important. Maintaining a low leakage current to keep both the passive power at a minimum and a reasonable I_{on}/I_{off} ratio ($\geq 10^4$ is typically desired in logic applications) is critical. Unipolar CNTFETs have I_{on}/I_{off} ratios in the range of 10^5–10^7.

The fact that Schottky barriers exist at CNT–metal interfaces does not imply that we have to be content with ambipolar behaviour and its implications. There are ways to further screen the Schottky barrier and get closer to a MOSFET-like bulk-switched device. Two different approaches have already been demonstrated. In one case, a double-gated CNT was used where the gates near the contacts selectively thinned the Schottky barriers, while a central gate was independently used to switch the bulk of the CNTFET (ref. 60). In this way, ambipolar behaviour and excess leakage current was eliminated and a sub-threshold slope of 60 mV per decade was achieved. As well as this electrostatic approach, chemical approaches have also been successful[61–63]. Substitutional doping of single-walled nanotubes using the traditional type of dopants such as B or P atoms has not been successful so far. This could be due to the large strain these impurities introduce to the CNT lattice. A different type of doping is produced by atoms or molecules that chemically adsorb on the CNT through a charge-transfer mechanism[61,62]. By selectively doping the contact regions of the CNTFET and using a central gate for switching, a bulk-like behaviour can be achieved. A further improvement of the sub-threshold slope of CNTFETs to values below the thermal limit was achieved, taking advantage of band-to-band tunnelling as a way of filtering the energy distribution of the electrons in CNTs. In this way S values of 40 mV per decade were obtained at room temperature[64].

Through the years a number of different CNTFET designs have been implemented, attempting to optimize their performance. For example, high-k materials have been used as gate insulators[65], wrap-around gates have been used to increase the coupling of the gate and the CNT channel, self-aligned designs and contact extensions to improve the device capacitance[61,66], and channel lengths have been scaled down to 18 nm (ref. 67).

In general, the key advantage of CNTFETs over Si MOSFETs in logic applications is their much lower capacitance of ~10 aF (for a $d_{CNT} = 1$ nm, $L = 10$ nm, $t_{ox} = 5$ nm device) and their somewhat lower operating voltage. Furthermore, the small size of the CNTs allows the fabrication of aligned arrays with high packing density. However, careful design and engineering are needed to make sure that the wire interconnect capacitance, typically ~0.2 aF nm^{-1}, does not overwhelm the capacitance of the CNT. It takes only about 50 nm of wiring for the interconnect to limit the capacitance of the 10 aF device. An area of clear advantage of CNTFETs is their lower switching energy per logic transition. The dynamic switching energy of a device is given by: $1/2(C_{dev}+C_{wire})V^2$, where C_{dev} and C_{wire} are the device and wiring capacitance contributions, respectively. To minimize the switching energy, minimum-sized devices, and interconnects should be used as well as the minimum supply voltage. Then the CNT can have a considerable advantage, of up to a factor of six, because of its smaller intrinsic capacitance and size[68].

ALTERNATING CURRENT PERFORMANCE OF CNTFETS

Although most of the work on CNTFETs has concentrated so far on their d.c. properties, the a.c. properties are technologically most relevant. Theoretically, it is predicted that a short nanotube operating in the ballistic regime, and the quantum capacitance limit should be able to provide gain in the THz range[69]. However, directly measuring the a.c. performance of a nanostructure such as a single nanotube is very difficult as the input impedance of a CNTFET is much higher than 50 Ω and the capacitance is typically in the aF range. A different approach is to operate the CNTFET as a mixer or rectifier[70,71–73]. Because of the nonlinear I–V characteristics of the transistor, an a.c. signal applied to the source becomes rectified and leads to a measurable d.c. current change. Using this approach, it was recently demonstrated that it is possible to obtain mixing up to a frequency of 50 GHz (ref. 72). As the authors pointed out, this is by no means the limit of performance of CNTFETs. The observed behaviour was determined by the parasitic capacitances of their system. This again underscores the need for a global optimization of a circuit before the unique properties of the nanotube can be effectively utilized.

NANOTUBE INTEGRATED CIRCUITS

The fabrication and evaluation of CNT-based devices has advanced beyond single devices to include logic gates[65,74–77] and, more recently more complex structures such as ring oscillators have been fabricated[78]. To build these circuits the energy efficient CMOS (complementary-MOS) architecture is preferred. This involves pairs of n- and p-type transistors. CNTs, where the valence and conduction bands are mirror images of each other (equal effective masses for

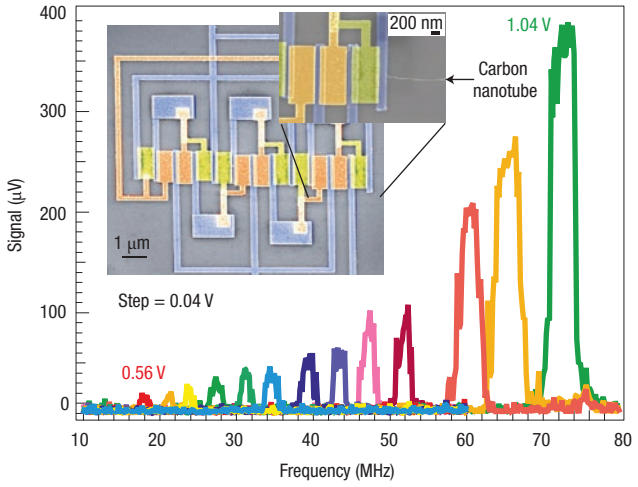

Figure 5 Ring-oscillator circuit based on a single nanotube. Scanning electron microscope image of the single nanotube, 5-stage ring-oscillator. The graph shows how the ringing frequency changes as the supply voltage is increased from 0.56 V to 1.04 V in 0.04 V steps.

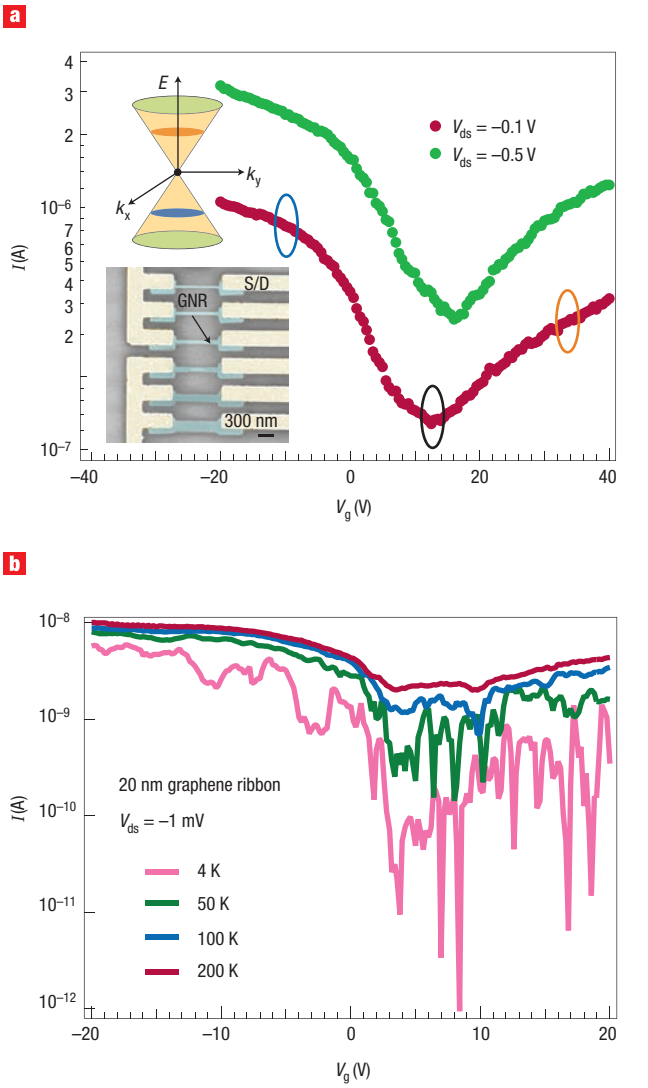

Figure 6 Graphene nanoribbon transistors. **a**, Current versus gate voltage characteristics of a 20 nm width graphene nanoribbon FET at room temperature. V_{ds} = –0.1 V (red) and –0.5 V (green). The blue, black and orange states represent, in the current versus gate voltage curves, the hole branch, minimum current, and electron branch, respectively. The insets show linear energy dispersion around the Dirac point, and the scanning electron microscope image of wired graphene nanoribbons of variable width produced by electron-beam lithography and etching. The widths of the ribbons are 20 nm (top), 30 nm, 40 nm, 50 nm, 100 nm and 200 nm (bottom). **b**, Temperature dependence of the current versus gate voltage characteristics of the 20 nm graphene nano-ribbon FET. V_{ds} = –1 mV. T = 4 K, 50 K, 100 K and 200 K.

electrons and holes) are ideally suited for such applications. The two types (p- and n-) of FETs can be made by doping the CNTs as discussed above. However, controlling doping in nanoscale devices is difficult. Fluctuations in the number and position of the dopants can have a profound effect on device performance. It has been shown recently, however, that the ambipolar behaviour of an undoped CNT can be successfully utilized to implement the CMOS architecture. A CMOS inverter is formed with a pair of p- and n- transistors operating under conditions where one FET is fully turned on while the other one is off. The ambipolar characteristics of a CNFET provide a pair of p- and n-type branches; however, the leakage branch of one type always has a comparable current level to the main branch (on-current) of the other. Therefore, obtaining control of the threshold voltage in an ambipolar device is not only important to match the desired supply voltage window, but is also critical to achieve a pair of p- and n-type characteristics which are suitable for CMOS logic.

For a given undoped CNFET with a fixed energy gap and oxide thickness, tuning the work function of the gate metal is the only way to control the threshold voltage. The gate work function acts like an extra voltage source in addition to the applied gate voltage. When the work functions are properly selected, the two characteristics can be relatively shifted towards each other and this leads to a distinguishable on-state in one and an off-state in the other. Fig. 5 shows scanning electron microscope image of the most complex structure so far based on a single carbon nanotube. It is a ring oscillator using Pd gates for p-FETs and Al gates for n-FETs. The frequency response from the ring oscillator shows a strong dependence on the supply voltage. A 72 MHz frequency is measured for a supply voltage of about 1 V. The small measured signal is due to the mismatch between the high output impedance of the nanotube circuit and the low input impedance of the measurement set-up. This impedance mismatch is a general problem of nanocircuits that needs to be addressed.

SWITCHING OF GRAPHENE NANORIBBONS

Having zero gap, graphene cannot be used directly in applications such as FETs for logic applications as the transistor cannot be turned completely off. Although the density of states at the Dirac point is zero, graphene has a minimum conductivity when the Fermi level is aligned with it that is found experimentally to be of the order of e^2/h (ref. 5,79–83). However, as we already discussed earlier, in addition to the 2D confinement in the plane of graphene, the graphene electrons (or holes) can be further confined by forming narrow ribbons and thus open a gap[4,11–13].

Very recently, electron-beam lithography and etching techniques have been used to introduce confinement to the 2D graphene[11,12]. The dependence of the transport properties on the ribbon width has been studied, and the energy gap that was opened up was indeed found to be inversely proportional to the ribbon width[12]. The smallest ribbon

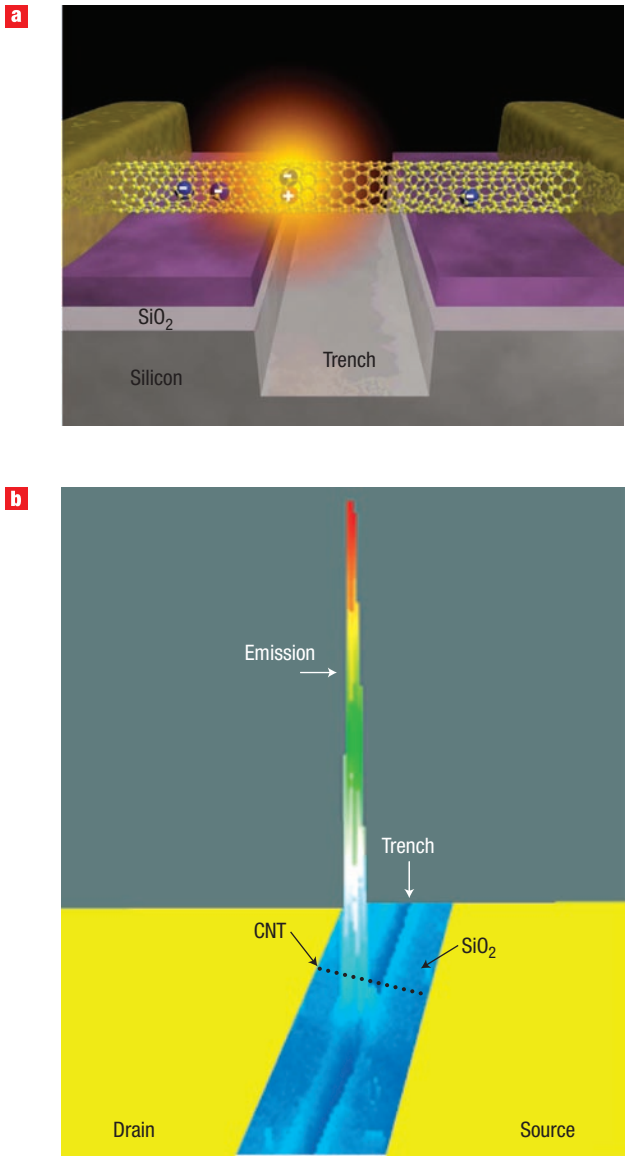

Figure 7 Light emission from a nanotube. **a**, Schematic of a modified ('trenched'), back-gated nanotube transistor used to produce a sudden change in the potential along the nanotube. **b**, Optical image of the trench and of the light emitted at its edge.

reproducibly defined by lithography is about 20 nm, shown in Fig. 6a, and induces the opening of a confinement gap of about 30 meV (ref. 11). At room temperature, this is too small a gap to have an observable effect on modulation of the current by the gate voltage, as shown in Fig. 6b. The GNR channel exhibits resistivity modulation by the gate voltage, which causes a significant Fermi-level shift (see inset of Fig. 6a). However, when the temperature is sufficiently lowered, the confinement gap starts to impede carrier injection and the device shows a clear on/off ratio as a normal semiconductor (Fig. 6b). Strong current fluctuations are observed at low temperatures for narrow ribbons, which is an indication of electron–electron interactions. Interestingly, no dependence on cutting angle of the graphene ribbon was observed experimentally[12]. This is likely the result of the present limitations of lithography rather than an intrinsic feature of graphene ribbon. State-of-the-art lithographic technology does not allow the formation of a uniquely defined ribbon edge, for example, armchair or zigzag, but a mixture of such edges may co-exist along the length of the graphene ribbon.

The possible existence of zigzag edges in graphene ribbons leads to localized edge states at the Fermi level[14,84]. Further complications could arise from the fact that cutting a ribbon leaves behind carbon dangling bonds that need to be saturated. Depending on the nature of the saturating group, the bonding and the potential at the edges are different from those in the bulk of the GNR. The combination of these factors could lead to a degradation of the mobility of the carriers by edge scattering, while the role of contact barriers will increase as scaling of the dimensions of the GNR proceeds. A general resistivity increase trend has been experimentally observed when the ribbon gets smaller than about 50 nm (ref. 11). More thorough studies are needed to find out the key contributors to this effect and possible ways to preserve the high mobility nature of the 2D graphene.

As in the case of CNTs, further confinement from two dimensions to quasi-zero-dimensions has recently been achieved on graphene[13]. A combined Coulomb blockade and confinement gap in a 10 nm island reaches ~$10k_BT$ at room temperature. This large gap makes it possible to operate it as a single electron transistor at room temperature. However, the challenge still remains of how to gain precise control of the graphene size and shape to obtain reproducible characteristics among different devices.

NANOTUBE OPTOELECTRONIC DEVICES

Electrically or optically generated electron and hole carriers in semiconductors can recombine by a variety of different mechanisms (direct or indirect recombination). In most cases, the recombination energy will be released as heat (phonons), but a fraction of the recombination events may involve the emission of a photon. This light-emission process is called 'electroluminescence' and is extensively used to produce solid-state light sources such as light emitting diodes (LEDs).

In order to fabricate LEDs, or other electroluminescent devices, one must generate and bring together significant populations of electrons and holes. Conventionally, this is achieved at the interface between a hole-doped and an electron-doped semiconductor (a p–n junction). As we have seen above, however, in ambipolar CNTFETs, by applying the appropriate biases, both electrons and holes can be simultaneously injected from the source and drain of the CNTFET. The quasi-1D character of the CNT confines the two types of carriers, which are driven towards each other. Indeed, radiative recombination in an ambipolar CNTFET was reported in ref. 85. Although the mechanism of that emission is similar to that of an LED, there is an important difference: the CNT is not doped so there is no clear p–n junction. As a result, the light does not originate from a fixed point along the CNT, but its origin can be translated by simply changing V_g, which determines the local potential in a long CNT device[85,86]. The overall emission intensity is maximized when the hole and electron currents become equal, which as we already indicated, occurs when $V_g = V_{ds}/2$. The emitted light is, as expected, polarized along the tube axis and the spectrum is, within the resolution of the measurements, the same as the photoluminescence spectrum of nanotubes with the same diameter.

In addition to this 'mobile' emission, localized electroluminescence is also observed from particular spots on a SWNT even under unipolar transport conditions. As light generation by radiative recombination requires that both types of carriers are present, we must conclude that at these spots electron–hole pairs are actively generated. Our studies showed that light-generating spots include a variety of inhomogeneities such as trapped charges in the gate insulator of the FET and interfaces between materials with different dielectric constants. In general these inhomogeneities produce voltage drops (electrical resistance) along the CNT and

generate large, local electric fields[87]. These fields can accelerate the carriers to an energy that allows them to generate electron–hole pairs through an intra-nanotube impact-excitation process. This excitation mechanism offers a number of possibilities for new applications. For example, more intense and brighter light sources can be produced because unipolar currents in CNTs can be higher than ambipolar currents, carrier multiplication can take place in the high fields and the emission is more localized. Furthermore, the excitation is not limited by dipole selection rules as photoexcitation is, and a number of different states can be populated.

This approach to generating high densities of excitations in low-dimensional systems can be used to resolve problems of current interest such as their mutual interactions and boson condensation. Recent work illustrates one way the impact excitation may be implemented in an LED[37]. A CNTFET was modified as shown in Fig. 7 to induce a sharp discontinuity in the potential; that is, to produce a waterfall-like energy landscape along the CNT channel. Electrons that are accelerated at the discontinuity can acquire enough energy to exceed the impact-excitation threshold and generate a bright light emitter with a yield that is about 1,000 times higher than that produced by recombination in an ambipolar CNTFET (Fig. 7)[37]. Another use of the localized electroluminescence can be as a much-needed analytical tool for identifying defects in either the CNT itself or the gate insulator. Parallel measurements of the mobile and localized electroluminescence of the CNTFETs and their I–V characteristics can provide unique information regarding the effect of specific defects and inhomogeneities on the electrical transport in CNTs.

Photoconductivity is the reverse process of electroluminescence, with optical radiation producing electron–hole pairs that are separated by the applied field. Single CNT photoconductivity was reported for the first time in 2003 (ref. 88). An example of such a measurement is shown in Fig. 8 (ref. 89). The resonant excitation of a CNT generates an electric current and can be used as a nanosized photodetector, a photo switch, or as a spectroscopic tool. Alternatively, in the open-circuit configuration the device generates a photovoltage. Internal fields such as those formed at Schottky contacts, or defect sites can also separate photogenerated electron–hole pairs and can be used to image such sites and determine the band bending in an open-circuit configuration[90–92]. Thus, a CNTFET device can be used as a transistor, a light emitter or a light detector[18]. Choosing between these different modes of operation only requires changes in the electrical inputs.

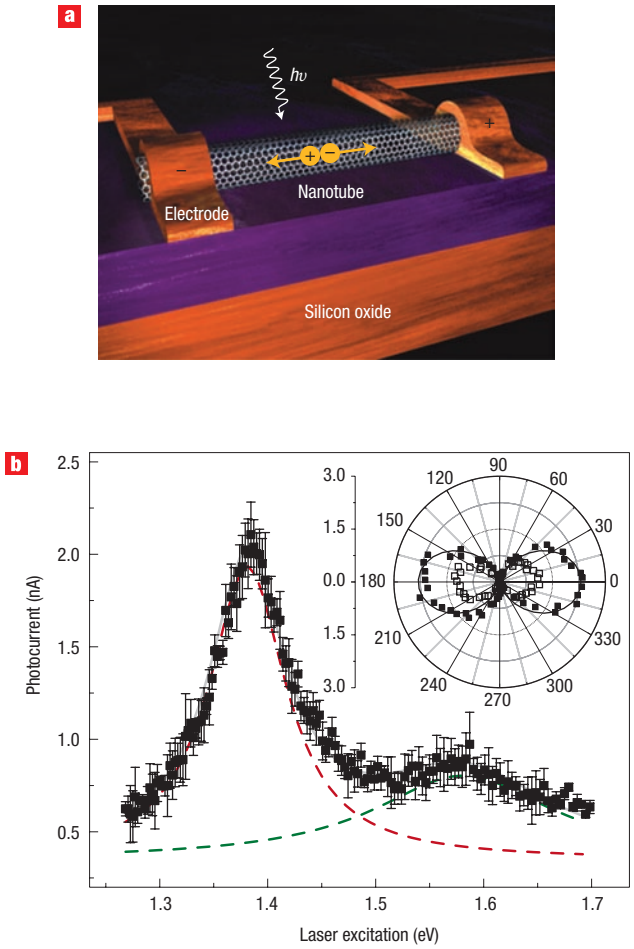

Figure 8 Photoconductivity with a nanotube. **a**, Schematic of a photoconductivity experiment. **b**, Induced photocurrent in a CNTFET as a function of the energy of the incident light. The strong peak corresponds to the second allowed exciton transition of the nanotube (E_{22} excitation); the weaker peak corresponds to the simultaneous excitation of one quantum of the G-phonon mode of the nanotube. The inset shows that both transitions are polarized along the nanotube axis.

THE FUTURE

Carbon nanotubes have provided us with an ideal model system to study electrical and optical phenomena on the nanometre scale. 1D materials with their exotic properties, long the realm of theoretical studies, are now open to experimentation. New states of condensed matter such as the Luttinger-Tomonaga liquid can be studied. Graphene is a novel, covalent 2D system that has already been found to exhibit a number of unique phenomena such as anomalous quantum Hall effect, Klein paradox and so forth. There is no doubt that in the future we will continue to obtain new information on the physics of the nanoscale through the study of nanotubes and graphene. Nanotube and graphene research is also teaching us how to handle and process nanomaterials and develop nanotechnology in general. In terms of direct technological applications, we focused here, because of limited space, only on electronic switching and light emission/detection. Nanotubes offer the potential of very fast (THz) transistors, ultimately scaled logic devices, and simpler and cheaper self-assembly based fabrication. In addition, transistors with properly functionalized CNTs can and are already being used as sensitive and selective chemical and biosensors. CNT-based nano-light sources and detectors may allow intra-chip optical communications and individual molecule level spectroscopy. The excellent electrical conduction of metallic CNTs may eventually allow the development of electronic systems where both active devices and interconnects are based on the same material — CNTs. Further integration to include optics could lead to a unified electronic — optoelectronic technology.

Graphene nanoribbons have field-switching capabilities, unlike graphene, in which the field switching is limited owing to its semi-metallic nature. The limited I_{on}/I_{off} of graphene field-effect devices may inhibit their application in computer logic, but may be appropriate for RF applications. Evidence, however, has been presented recently that bilayer graphene can provide a sizable and field-tuneable bandgap and as such may provide the basis of novel field-effect electronic and optoelectronic devices[93,94] A gate-controlled p–n junction has also been demonstrated in graphene, and used to further explore the quantum Hall effect[95,96]. The large electronic and spin coherence lengths of both materials could also lead to quantum interference and spintronic devices. Spin-polarized injection can be achieved using manganite electrodes. The weak spin-orbit coupling and short transit times of carriers in nanotubes tend to preserve the spin polarization and can lead to high $\Delta V/V$ ratios, where V is the bias voltage and ΔV its variation when the magnetic configuration is changed[97]. Spin transport

and spin precession over micrometre-scale distances have also been demonstrated in single graphene sheets at room temperature[98].

How soon do we expect to see these developments? What is the bottleneck in the development of nanotubes, graphene and indeed in any high-end nanotechnology? The main hurdle is our current inability to produce large amounts of identical nanostructures. Nanotubes come in many sizes and structures and the same is true of many other nanostructures. For example, there is no reliable way to directly produce a single CNT type such as will be needed in a large integrated system, and patterning graphene is limited by the resolution of current lithographic techniques. However, promising signs that these problems will be circumvented soon are appearing. Already, separation of single-type nanotubes from mixtures has been achieved, and direct growth of graphene is possible. Similarly encouraging results are being reported in the area of self-assembly of CNT devices.

doi:10.1038/nnano.2007.300

Published online: 30 September 2007.

References

1. Avouris, P. Electronics with carbon nanotubes. *Phys. World* **20,** 40–45 (March 2007).
2. Wallace, P. R. The band theory of graphite. *Phys. Rev.* **71,** 622–634 (1947).
3. Novoselov, K. S. *et al.* Electric field effect in atomically thin carbon films. *Science* **306,** 666–669 (2004).
4. Berger, C. *et al.* Electronic confinement and coherence in patterned epitaxial graphene. *Science* **312,** 1191–1196 (2006).
5. Novoselov, K. S. *et al.* Two-dimensional gas of massless Dirac fermions in graphene. *Nature* **438,** 197–200 (2005).
6. Zhang, Y., Tan, Y.-W., Stormer, H. L. & Kim, P. Experimental observation of the quantum Hall effect and Berry's phase in graphene. *Nature* **438,** 201–204 (2005).
7. Novoselov, K. S. *et al.* Room-temperature quantum Hall effect in graphene. *Science* **315,** 1379 (2007).
8. Saito, R., Dresselhaus, G., & Dresselhaus, M. S. (eds.) Physical properties of carbon nanotubes. (Imperial College Press, London, 1998)
9. Anantram, M. P. & Leonard, F. Physics of carbon nanotube electronic devices. *Rep. Prog. Phys.* **69,** 507–561 (2006).
10. Charlier, J.-C., Blase, X., & Roche, S. Electronic and transport properties of nanotubes. *Rev. Mod. Phys.* **79,** 677–733 (2007).
11. Chen, Z., Lin, Y.-M., Rooks, M. J., & Avouris, P. Graphene nano-ribbon electronics. Preprint at <http://arxiv.org/abs/cond-mat/0701599> (2007).
12. Han, M. Y., Özyilmaz, B., Zhang, Y., & Kim, P. Energy band gap engineering of graphene nanoribbons. *Phys. Rev. Lett.* **98,** 206805 (2007).
13. Geim, A. K. & Novoselov, K. S. The rise of graphene. *Nature Mater.* **6,** 183–191 (2007).
14. Nakada, K., Fujita, M., Dresselhaus, G., & Dresselhaus, M. S. Edge state in graphene ribbons: Nanometer size effect and edge shape dependence. *Phys. Rev. B* **54,** 17954–17961 (1996).
15. Son, Y.-W., Cohen, M. L., & Louie, S. G. Energy gaps in graphene nanoribbons. *Phys. Rev. Lett.* **97,** 216803 (2006).
16. Barone, V., Hod, O. & Scuseria, G. E. Electronic structure and stability of semiconducting graphene nanoribbons. *Nano Lett.* **6,** 2748–2754 (2006).
17. White, C. T., Li, J., Gunlycke, D. & Mintmire, J. W. Hidden one-electron interactions in carbon nanotubes revealed in graphene nanostrips. *Nano Lett.* **7,** 825–830 (2007).
18. Avouris, P. *et al.* Carbon nanotube optoelectronics. P*hysica Status Solidi B* **243,** 3197–3203 (2006).
19. Landauer, R. Spatial variation of currents and fields due to localized scatterers in metallic conduction. *IBM J. Res. Dev.* **32,** 306 (1988).
20. Büttiker, M. Symmetry of electrical conduction. *IBM J. Res. Dev.* **32,** 317 (1988).
21. Ilani, S., Donev, L. A. K., Kindermann, M. & McEuen, P. L. Measurement of the quantum capacitance of interacting electrons in carbon nanotubes. *Nature Phys.* **2,** 687–691 (2006).
22. Burke, P. An RF circuit model for carbon nanotubes. *IEEE Trans. Nanotechnol.* **2,** 55–58 (2003).
23. Ando, T. & Nakanishi, T. Impurity scattering in carbon nanotubes — absence of backscattering. *J. Phys. Soc. Jpn.* **67,** 1104–1113 (1998).
24. White, C. T. & Todorov, T. N. Carbon nanotubes as long ballistic conductors. *Nature* **393,** 240–242 (1998).
25. Klein, O. An introduction to Kaluza-Klein theories. *Z. Phys.* **37,** 895 (1926).
26. Katsnelson, M. I., Novoselov, K. S. & Geim, A. K. Unconventional quantum Hall effect and Berry's phase of 2π in bilayer graphene. *Nature Phys.* **2,** 177–180 (2006).
27. Perebeinos, V., Tersoff, J. & Avouris, P. Electron-phonon interaction and transport in semiconducting carbon nanotubes. *Phys. Rev. Lett.* **94,** 086802 (2005).
28. Zhou, X., Park, J-Y, Huang, S., Liu, J. & McEuen, P. L. Band structure, phonon scattering, and the performance limit of single-walled carbon nanotube transistors. *Phys. Rev. Lett.* **95,** 146805 (2005).
29. Ashcroft, N. W. & Mermin, N. D. *Solid State Physics* (Saunders, 1976).
30. Durkop, T., Getty, S. A., Cobas, E., & Fuhrer, M. S. Extraordinary mobility in semiconducting carbon nanotubes. *Nano Lett.* **4,** 35–39 (2004).
31. Perebeinos, V., Tersoff, J. & Avouris, P. Mobility in semiconducting carbon nanotubes at finite carrier density. *Nano Lett.* **6,** 205–208 (2006).
32. Yao, Z., Kane, C. L. & Dekker, C. High-field electrical transport in single-wall carbon nanotubes. *Phys. Rev. Lett.* **84,** 2941–2944 (2000).
33. Javey, A. *et al.* High-field quasiballistic transport in short carbon nanotubes. *Phys. Rev. Lett.* **92,** 106804 (2004).
34. Park, J. Y. *et al.* Electron-phonon scattering in metallic single-walled carbon nanotubes. *Nano Lett.* **4,** 517–520 (2004).
35. Chen, Y.-F. & Fuhrer, M. S. Electric-field-dependent charge-carrier velocity in semiconducting carbon nanotubes. *Phys. Rev. Lett.* **95,** 236803 (2005).
36. Pennington, G. & Goldsman, N. Semiclassical transport and phonon scattering of electrons in semiconducting carbon nanotubes. *Phys. Rev. B* **68,** 045426 (2003).
37. Chen, J. *et al.* Bright infrared emission from electrically induced excitons in carbon nanotubes. *Science* **310,** 1171–1174 (2005).
38. Perebeinos, V. & Avouris, P. Impact excitation by hot carriers in carbon nanotubes. *Phys. Rev. B* **74,** 121410R (2006).
39. Ando, T. J. Excitons in carbon nanotubes. *J. Phys. Soc. Jpn* **66,** 1066–1073 (1997).
40. Spataru, C. D., Ismail-Beigi, S., Benedict, L. X. & Louie, S. G. Excitonic effects and optical spectra of single-walled carbon nanotubes. *Phys. Rev. Lett.* **92,** 077402 (2004).
41. Perebeinos, V., Tersoff, J. & Avouris, P. Scaling of excitons in carbon nanotubes. *Phys. Rev. Lett.* **92,** 257402 (2004).
42. Pop, E. *et al.* Negative differential conductance and hot phonons in suspended nanotube molecular wires. *Phys. Rev. Lett.* **95,** 155505 (2005).
43. Lazzeri, M., Pisanec, S., Mauri, F., Ferrari, A. C. & Robertson J. Electron transport and hot phonons in carbon nanotubes. *Phys. Rev. Lett.* **95,** 236802 (2005).
44. Collins, P. G., Arnold, M. S. & Avouris, P. Engineering carbon nanotubes and nanotube circuits using electrical breakdown. *Science* **292,** 706–709 (2001).
45. Collins, P. G. Hersam, M., Arnold, M., Martel, R. & Avouris, P. Current saturation and electrical breakdown in multiwalled carbon nanotubes. *Phys. Rev. Lett.* **86,** 3128–3131 (2001).
46. Naeemi, A., Sarvati, R. & Meindl, J. D. Performance comparison between carbon nanotube and copper interconnects for GSI. *IEDM Digest* 699–702 (2004).
47. Tans, S. J., Verscheuren, A. R. M. & Dekker, C. Room-temperature transistor based on a single carbon nanotube. *Nature* **393,** 49–52 (1998).
48. Martel, R., Schmidt, T, Shea, H. R., Hertel, T. & Avouris, P. Single- and multi-wall carbon nanotube field-effect transistors. *Appl. Phys. Lett.* **73,** 2447–2449 (1998).
49. Sze, S. M. *Physics of Semiconductor Devices*. (Wiley, New York, 1981).
50. Appenzeller, J., Knoch, J., Radosavljević, M. & Avouris, P. Multimode transport in Schottky-barrier carbon-nanotube field-effect transistors. *Phys. Rev. Lett.* **92,** 226802 (2004).
51. Léonard, F. & Tersoff, J. Role of Fermi-level pinning in nanotube Schottky diodes. *Phys. Rev. Lett.* **84,** 4693–4696 (2000).
52. Martel, R. *et al.* Ambipolar electrical transport in semiconducting single-wall carbon nanotubes. *Phys. Rev. Lett.* **87,** 256805 (2001).
53. Heinze, S. *et al.* Carbon nanotubes as Schottky barrier transistors. *Phys. Rev. Lett.* **89,** 106801 (2002).
54. Appenzeller, J. *et al.* Field-modulated carrier transport in carbon nanotube transistors. *Phys. Rev. Lett.* **89,** 126801 (2002).
55. Javey, A. *et al.* Ballistic carbon nanotube field-effect transistors. *Nature* **424,** 654–657 (2003).
56. Appenzeller, J., Radosavljevi, M., Knoch, J. & Avouris, P. Tunneling versus thermionic emission in one-dimensional semiconductors. *Phys. Rev. Lett.* **92,** 048301 (2004).
57. Chen, Z., Appenzeller, J. Knoch, J., Lin, Y-M & Avouris, P. The role of metal-nanotube contact in the performance of carbon nanotube field-effect transistors. *Nano Lett.* **5,** 1497–1502 (2005).
58. Radosavljevic, M., Heinze, S., Tersoff, J. & Avouris, P. Drain voltage scaling in carbon nanotube transistors. *Appl. Phys. Lett.* **83,** 2435–2437 (2003).
59. Avouris, P. Carbon nanotube electronics. *Proc. IEEE* **91,** 1772–1784 (2003).
60. Lin, Y.-M., Appenzeller, J., Knoch, J. & Avouris, P. High-performance carbon nanotube field-effect transistor with tunable polarities. *IEEE Trans. Nanotechnol.* **4,** 481–489 (2005).
61. Chen, J., Klinke, C., Afzali, A. & Avouris, P. Self-aligned carbon nanotube transistors with charge transfer doping. *Appl. Phys. Lett.* **86,** 123108 (2005).
62. Klinke, C., Chen, J., Afzali, A. & Avouris, P. Charge transfer induced polarity switching in carbon nanotube transistors. *Nano Lett.* **5,** 555–558 (2006).
63. Javey, A. *et al.* High performance n-type carbon nanotube field-effect transistors with chemically doped contacts. *Nano Lett.* **5,** 345–348 (2005).
64. Appenzeller, J., Lin, Y.-M., Knoch, J. & Avouris, P. Band-to-band tunneling in carbon nanotube field-effect transistors. *Phys. Rev. Lett.* **93,** 196805 (2004).
65. Javey, A. *et al.* High-k dielectrics for advanced carbon nanotube transistors and logic gates. *Nature Mater.* **1,** 241–246 (2002).
66. Javey, A. *et al.* Self-aligned ballistic molecular transistors and electrically parallel nanotube arrays. *Nano Lett.* **4,** 1319–1322 (2004).
67. Seidel, R. V. *et al.* Sub-20 nm short channel carbon nanotube transistors. *Nano Lett.* **5,** 147–150 (2005).
68. Solomon, P. M. in *Future Trends in Microelectronics: Up the Nano Creek* (eds Luryi, S., Xu, J. M., & Zaslavsky, A.) 212–223 (Wiley, New York, 2007).
69. Castro, L. C. *et al.* Method for predicting f_T for carbon nanotube FETs. *IEEE Trans. Nanotechnol.* **4,** 699–704 (2005).
70. Frank, D. J. & Appenzeller, J. High frequency response in carbon nanotube field-effect transistors. *IEEE Electron. Device Lett.* **25,** 34–36 (2004).
71. Li, S. D., Yu, Z., Yen, S-F, Tang, W. C. & Burke, P. J. Carbon nanotube transistor operation at 2.6 GHz. *Nano Lett.* **4,** 753–756 (2004).
72. Rosenblatt, S., Lin, H., Sazonova, V., Tiwari, S. & McEuen, P. L. Mixing at 50GHz using a single-walled carbon nanotube transistor. *Appl. Phys. Lett.* **87,** 153111–15313 (2005).
73. Bethoux, J.-M. *et al.* An 8-GHz f_t carbon nanotube field-effect transistor for gigahertz range applications. *IEEE Electron. Device Lett.* **27,** 681–683 (2006).
74. Bachtold, A., Hadley, P., Nakanishi, T. & Dekker, C. Logic circuits with carbon nanotube transistors. *Science* **294,** 1317–1320 (2001).
75. Derycke, V., Martel, R., Appenzeller, J. & Avouris, P. Carbon nanotube inter- and intramolecular logic gates. *Nano Lett.* **1,** 453–456 (2001).
76. Liu, X., Lee, C., Zhou, C. & Han, J. Carbon nanotube field-effect inverters. *Appl. Phys. Lett.* **79,** 3329–3331 (2001).

77. Javey, A., Wang, Q., Ural, A., Li, Y. & Dai, H. Carbon nanotube transistor arrays for multistage complementary logic and ring oscillators. *Nano Lett.* **2,** 929–932 (2002).
78. Chen, Z. *et al.* An integrated logic circuit assembled on a single carbon nanotube. *Science* **311,** 1735 (2006).
79. Katsnelson, M. I. Minimal conductivity in bilayer graphene. *Eur. Phys. J. B* **51,** 157 (2006).
80. Gusynin, V. P. & Sharapov, S. G. Unconventional integer quantum hall effect in graphene. *Phys. Rev. Lett.* **95,** 146801 (2005).
81. Peres, N. M. R., Guines, F. & Neto, A. H. C. Electronic properties of disordered two-dimensional carbon. *Phys. Rev. B* **73,** 125411 (2006).
82. Tworzydo, J., Trauzettel, B., Titov, M., Rycerz, A. & Beenakker, C. W. J. Sub-Poissonian shot noise in graphene. *Phys. Rev. Lett.* **96,** 246802 (2006).
83. Ziegler, K., Robust transport properties in graphene. *Phys. Rev. Lett.* **97,** 266802 (2006).
84. Niimi, Y. *et al.* Scanning tunneling microscopy and spectroscopy of the electronic local density of states of graphite surfaces near monoatomic step edges. *Phys. Rev. B* **73,** 085421 (2006).
85. Misewich, J. A. *et al.* Electrically induced optical emission from a carbon nanotube FET. *Science* **300,** 783–786 (2003).
86. Freitag, M. *et al.* Mobile ambipolar domain in carbon-nanotube infrared emitters. *Phys. Rev. Lett.* **93,** 076803 (2004).
87. Freitag, M. *et al.* Electrically excited, localized infrared emission from single carbon nanotubes. *Nano Lett.* **6,** 1425–1433 (2006).
88. Freitag, M. *et al.* Photoconductivity of single carbon nanotubes. *Nano Lett.* **3,** 1067–1071 (2003).
89. Qiu, X., Freitag, M., Perebeinos, V. & Avouris, P. Photoconductivity spectra of single carbon nanotubes: Implications on the nature of their excited states. *Nano Lett.* **5,** 749–752 (2005).
90. Balasubramanian, K *et al.* Photoelectronic transport imaging of individual semiconducting carbon nanotubes. *Appl. Phys. Lett.* **84,** 2400–2402 (2004).
91. Freitag, M. *et al.* Imaging of the Schottky barriers and charge depletion in carbon nanotube transistors. *Nano Lett.* **7,** 2037–2042 (2007).
92. Freitag, M. *et al.* Scanning photovoltage microscopy of potential modulations in carbon nanotubes. *Appl. Phys. Lett.* **91,** 031101 (2007).
93. Castro, E. V. *et al.* Biased bilayer graphene: semiconductor with a gap tunable by electric field effect. Preprint at < http://arxiv.org/abs/cond-mat/0611342 > (2006).
94. Ohta, T. *et al.* Controlling the electronic structure of bilayer graphene. *Science* **313,** 951–954 (2006).
95. Williams, J. R., DiCarlo, L. & Marcus, C. M. Quantum Hall effect in a gate-controlled p-n junction of graphene. *Science* **317,** 638–641 (2007).
96. Abanin, D. A. & Levitov, L. S. Quantized transport in graphene p-n junctions in a magnetic field. *Science* **317,** 641–643 (2007).
97. Hueso, L. E. *et al.* Transformation of spin information into large electrical signals using carbon nanotubes. *Nature* **445,** 410–413 (2007).
98. Tombros, N., Jozsa, C., Popinciuc, M., Jonkman, H. T. & van Wees, B. J. Electronic spin transport and spin precession in single graphene layers at room temperature. *Nature* **448,** 571–574 (2007).